ISSN 2616-5767 Vol.6, Issue 11: 70-81, DOI: 10.25236/AJETS.2023.061111

Enhancing SRTM DEM Correction Accuracy with a PSO-RF Method Utilizing ICESat-2/ATLAS Data

Zeyuan Dai[1], Xiang Liu[2], Lihua Zhang[1,*], Yinfei Zhou[1], Zeyu Li[3]

[1]Department of Military Oceanography and Hydrography & Cartography, Dalian Naval Academy, Dalian, 116018, China
[2]Chart Information Center, Tianjin, 116018, China
[3]Troops 91937, Ningbo, 315000, China
[*]Corresponding author: zlhua@163.com

Abstract: *This study proposes a new method for correcting the Shuttle Radar Topography Mission (SRTM) digital elevation model (DEM), as current methods, such as the polynomial regression (PR) method, are limited in their ability to fully capture complex nonlinear relationships between elevation errors and their influencing factors. The proposed method combines the benefits of particle swarm optimization (PSO) and random forest (RF) algorithms. First, elevation control photons (ECPs) are extracted from strong beams of the Advanced Topographic Laser Altimeter System (ATLAS) on the Ice, Cloud, and land Elevation Satellite-2 (ICESat-2), and the elevation errors of the SRTM DEM, terrain factors, and landcover classes for each ECP are then calculated. Next, a SRTM DEM correction model based on the RF is designed, and PSO is utilized to determine hyper-parameters of the RF. Finally, the corrected SRTM DEM for the San Joaquin Valley and the Sierra Nevada is produced as an example. The proposed PSO-RF correction method is validated using high-precision airborne light detection and ranging (LiDAR) data, and the results show that it significantly improves the quality of the SRTM DEM. Specifically, the mean absolute error (MAE) and root mean square error (RMSE) are 9.24% and 13.3% lower than those of the existing PR method in the study area, respectively.*

Keywords: *ICESat-2/ATLAS; SRTM DEM; random forest; particle swarm optimization; elevation error correction*

1. Introduction

The digital elevation model (DEM) is a digital representation of surface elevation, and it has become a vital input variable in a variety of research fields such as geomorphology [1], hydrology [2], terrain mapping [3], disaster monitoring and control [4,5], etc. To date, there are a series of global-scale, high-accuracy, and open-access DEM datasets derived from remote-sensing-based techniques. Among these datasets, the DEM from the Shuttle Radar Topography Mission (SRTM) is the most widely used because it has the most comprehensive evaluation in terms of coverage, accuracy, and accessibility. However, the precision of the SRTM DEM is affected by the observation means, terrain, landcover, and some other potential factors, and its elevation still has non-negligible errors despite several times of correction, and the elevation accuracy often varies greatly with different terrain and landcover.

In order to reduce the elevation error of SRTM DEM, scholars have tried various types of reference data with higher accuracy to evaluate and improve the quality of SRTM DEM, such as high-accuracy Global Navigation Satellite System (GNSS) measurement points [7], airborne LiDAR data [8, 9], high-quality DEM [10], etc. However, all the reference data mentioned above are limited in distribution and difficult to obtain and produce on a large scale, which makes it hard to correct the elevation error of the SRTM DEM on a global scale or in an arbitrary area according to the actual need. In 2003, the National Aeronautics and Space Administration (NASA) launched the Ice, Cloud, and land Elevation Satellite (ICESat) with a Geoscience Laser Altimeter System (GLAS). Due to its characteristics of near-global coverage and relatively high accuracy, the ICESat/GLAS data has been applied to the research of SRTM DEM correction. Du et al. established a one-dimensional linear regression model between ICESat/GLAS and SRTM DEM in typical high-elevation mountainous and low-elevation coastal plain areas of China to improve the elevation accuracy of SRTM DEM in specific regions [11]; Su et al. used ICESat/ATLAS as the reference data to correct the elevation errors of SRTM DEM based on tree height, canopy cover, and slope by developing a multiple linear regression model for the data in the vegetation-covered

ISSN 2616-5767 Vol.6, Issue 11: 70-81, DOI: 10.25236/AJETS.2023.061111

mountainous areas of the Sierra Nevada [12]; Qin et al. designed a spatial interpolation method to construct an error surface with the help of ICESat/GLAS data to correct the elevation errors of SRTM DEM [13]; Chen et al. compared some machine learning methods with the reference of ICESat/GLAS data and found that the random forest (RF) is the most proper model for the correction of the SRTM DEM [14], but the RF model is sensitive to the hyper-parameters. With the help of the ICESat/GLAS data, these works laid the groundwork for the acquisition of a more accurate corrected SRTM DEM. But ICESat expired in 2009, and its data stopped updating accordingly, which prevented the production of a more up-to-date corrected SRTM DEM.

In September 2018, the Ice, Cloud, and land Elevation Satellite-2 (ICESat-2) was successfully launched as the first laser altimetry satellite in the photonic regime, which carries an Advanced Topographic Laser Altimeter System (ATLAS) with the advantages of low energy, high sensitivity, and high repetition frequency. In comparison to ICESat/GLAS in the linear regime, ICESat-2/ATLAS can acquire elevation data with a smaller spot and a higher density. More importantly, the accuracy of ICESat-2/ATLAS data is also better than that of ICESat/GLAS in both horizon and elevation directions [15]. As a result, the ICE-Sat-2/ATLAS data can be used to create a more precise and up-to-date corrected SRTM DEM. On this basis, Magruder et al. used photons classified as ground from ICESat-2/ATLAS data as the reference and then combined them with Landsat-8 images to construct a polynomial regression (PR) equation to establish the correction of the SRTM DEM, and the accuracy of the corrected DEM was improved compared to the original data [16]. However, due to the complex nonlinear relationship between the error of the SRTM DEM and its influencing factors, the PR equation, which only a simple mathematical expression can hardly express adequately, and the accuracy of the SRTM DEM corrected by this method are still not stable enough, particularly in areas with complex terrain and landcover. Therefore, a RF-based model combined with particle swarm optimization (PSO) is proposed for the correction of the SRTM DEM. Firstly, the reference elevation control photons (ECPs) are extracted from the strong beams of the ICESat-2/ATLAS ATL03 data. Then, taking longitude and latitude, slope, aspect, relief, and landcover class as the response variables of the correction model, a PSO-RF model is designed. Finally, the model is trained using all of the ECPs that were collected to improve the accuracy of the SRTM DEM. Through experiments, the effectiveness of the proposed method was verified and compared with the existing PR method.

2. Materials

2.1. Study Area

The study area selected for this study is presented in Figure 1, situated in the region of the Sierra Nevada and San Joaquin Valley on the west coast of the United States. This study area is characterized by high mountains on the east side and plains on the west side, with a diversity of topography types and landcover classes, which can test the validity of the proposed PSO-RF method in this study in a more comprehensive way.

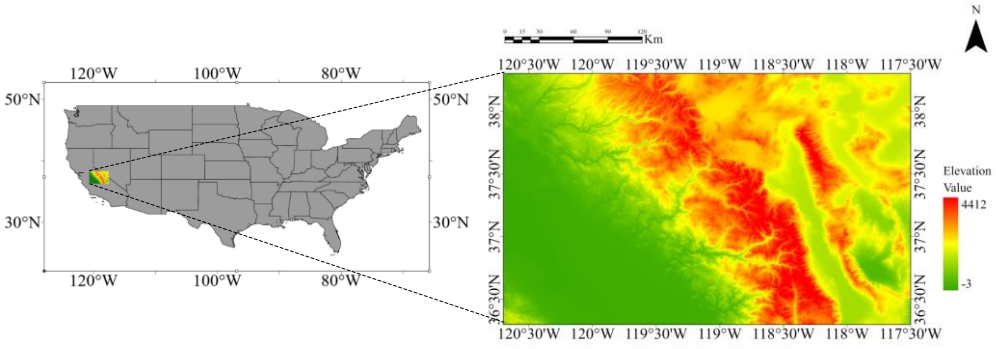

Figure 1: Location of study area.

2.2. SRTM DEM data

As mentioned above, the SRTM DEM is a near-global DEM product that was generated by a joint collaboration between NASA and the National Geospatial-Intelligence Agency (NGA). The SRTM DEM is obtained by the interferometric synthetic aperture radar (InSAR) technique using C-Band Space-borne

ISSN 2616-5767 Vol.6, Issue 11: 70-81, DOI: 10.25236/AJETS.2023.061111

Imaging Radar (C-SIR) and X-Band Synthetic Aperture Radar (X-SAR) sensors [17, 18]. It encompasses a latitude range of 56°S–60°N, which covers approximately 80% of the global land area. Since its release, the SRTM DEM has undergone several revisions, and the version of data used in our study is SRTMGL1, which has a resolution of 1″ (about 30 m) with the World Geodetic System 1984 (WGS-84) coordinate system as its geographic coordinate system and the geodetic level from the Earth Gravitational Model 1996 (EGM96) as its vertical datum. This version of SRTM DEM data integrates multi-source and multi-type reference DEM data, such as ASTER GDEM and USGS GMTED, and solves the problem of voids in some areas that existed in the previous version of SRTM DEM [6].

2.3. Globeland30 data

To obtain a more accurate surface coverage type, the GlobeLand30 (V2020) data in the study area was collected as the global land cover data used for the later experiment. The National Geomatics Center of China (NGCC) released this dataset, which makes use of images from multiple sources including Landsat, HJ-1 (China Environment and Disaster Reduction Satellite), and GF-1 (China High Resolution Satellite). The GlobalLand30 has the same spatial resolution as the SRTM DEM and includes 10 surface types such as arable land, forest land, grassland, and man-made surfaces. By sampling, it was shown that the overall accuracy of GlobeLand30 (V2020) is better than 85%, which means it can provide accurate surface coverage data to support the PSO-RF method in this study.

2.4. ICESat-2/ATLAS data.

The ATLAS on board ICESat-2 employs the micro-pulse multi-beam photon-counting laser LiDAR technology, which emits a laser beam at a repetitive frequency of 10 kHz and divides it into three pairs of laser sub-beams by diffractive optics, each pair containing both strong and weak beams. As shown in Figure 2, three pairs of laser beams are arranged in parallel in the along-track direction with a spacing of about 3 km in the cross-track direction, and the strong and weak beams in any sub-beam are separated by about 90 m in the cross-track direction and about 2.5 km in the along-track direction, with an energy ratio of 4:1 between the two, and each beam can be characterized as a surface spot with a diameter of about 17 m and a spacing of 0.7 m along the track [19]. The dataset of ICESat-2/ATLAS is divided into four levels (Level 0-Level 3) and subdivided into 21 products from ATL00 to ATL21 (without ATL05). Among these data, ATL03 is the geolocated photon product, which records the precise latitude and longitude as well as the geodetic height information relative to the reference ellipsoid for each photon. And ATL08 is the land and vegetation elevation data, which contains surface and canopy information such as slope, terrain height, and canopy height within every 100 m. Each signal photon in the ATL03 data is classified into three types: top-of-canopy, canopy, and ground, using the Differential, Regressive, and Gaussian Adaptive Nearest Neighbor (DRAGANN) noise-removing algorithm and iterative median filtering. This classified result is then written to the corresponding ATL08 data. Since the strong beam is better at inverting the terrain than the weak beam [20, 21], the proposed method only uses the photons that are classified as terrain in the strong beam as the elevation control photons. The distribution of these data is shown in Figure 3.

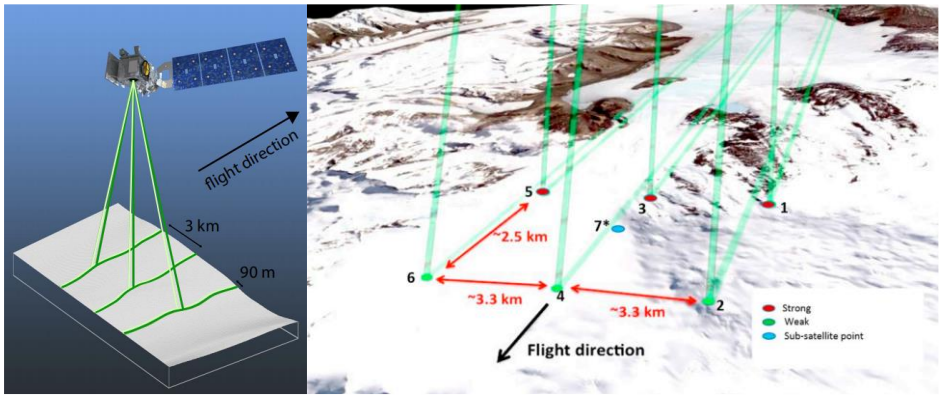

Figure 2: ICESat-2/ATLAS beams distribution sketch map [19].

ISSN 2616-5767 Vol.6, Issue 11: 70-81, DOI: 10.25236/AJETS.2023.061111

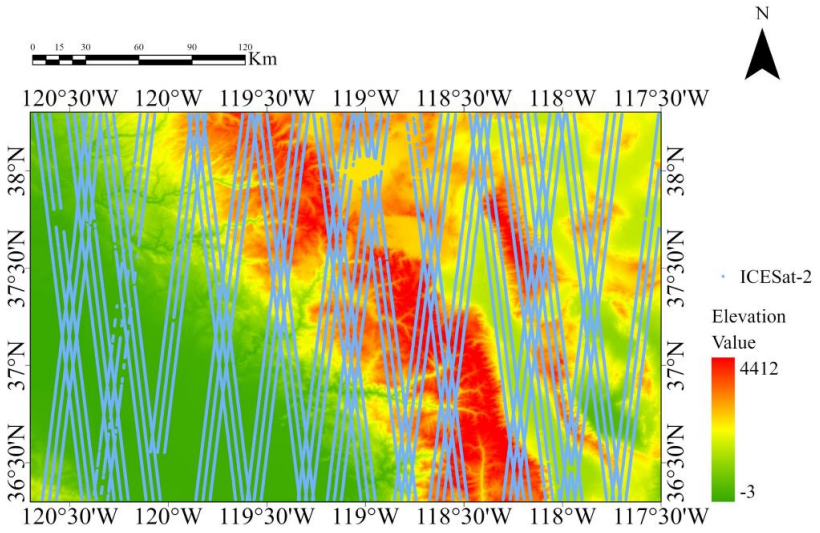

Figure 3: Distribution of ICESat-2/ATLAS data in the study area.

2.5. Airborne LiDAR data

To verify the actual performance of the corrected SRTM DEM, the high-accuracy airborne LiDAR-derived DEM data released by the National Ecological Observatory Network (NEON) with a resolution of 1 m is used as the validation data, and the distribution of this data can be seen in Figure 4. This data has an error better than 0.36 m and 0.40 m in the horizontal and vertical directions, respectively. The geographic coordinate system of this airborne LiDAR-derived DEM is WGS-84, while the vertical datum is the 1988 North American Vertical Datum (NAVD-88). For subsequent model design and verification results' accuracy, without special explanation, the VDatum software developed by the National Oceanic and Atmospheric Administration (NOAA) is used to finish all the coordinate and datum transformations in this study.

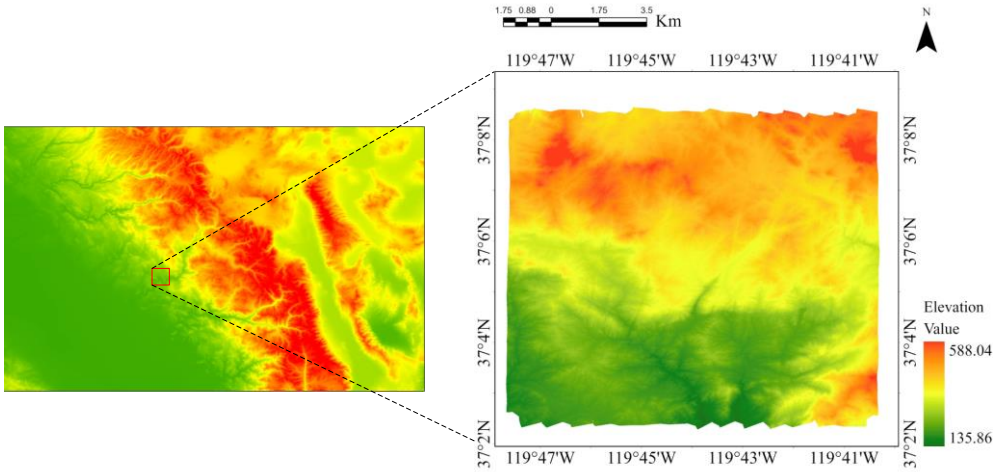

Figure 4: Distribution of LiDAR DEM.

3. Methods

3.1. Data Preprocessing

3.1.1. Elevation Control Photons Extraction

Based on the DRAGANN noise-removing algorithm and the photon classification results, the ICESat-2 scientific team provides a classification flag for each photon (named classed*_pc_flag*) in the ATL08 data, with the values 0, 1, 2, and 3 representing noise, ground, canopy, and top of canopy, respectively. Existing studies have shown that the DRAGANN algorithm performs better under low and medium

ISSN 2616-5767 Vol.6, Issue 11: 70-81, DOI: 10.25236/AJETS.2023.061111

signal-to-noise ratios (SNRs), while there may be some signal photons misclassified as noise photons under strong noise [22], resulting in wrong classification results and affecting the subsequent correction model. Therefore, the method in this study first roughly calculates the SNRs of ATL03 by using the signal photon confidence labels (named *signal_conf_ph*) in ATL03. The ground photons are extracted directly from ATL03 data with low and medium SNRs by associating the classification flag in ATL08 to ATL03 [20]. As for the ATL03 with low SNRs, the signal photons are obtained by the pruned quadtree denoising method [23] and then classified by an adaptive cloth simulation method to accurately extract the ground photons [24]. Finally, the ground photons in different noise backgrounds are integrated and used as ECPs for the subsequent correction of the SRTM DEM. It should be noted that since the elevation of the photon in the ATL03 is the ellipsoidal height with the WGS-84 reference ellipsoid, similar to the LiDAR DEM, the geodesic height of the photon relative to the ellipsoid is also converted to the EGM96 vertical datum.

3.1.2. Terrain Factors and Landcover Classes Extraction

The downloaded SRTM DEM is first cropped and mosaicked to obtain data for the study area, and the merged DEM is then processed using ArcGIS to calculate the terrain factors, including slope, aspect, and relief data, and the terrain factors at the location ECPs are finally extracted using bilinear interpolation.

For the extraction of landcover, since Globeland30 uses Universal Transverse Mercator (UTM) projection with 6° zoning and the study area of this study spans the 10th and 11th projection zones, the geographic coordinate system of ECPs is first projected to the UTM Zone 10N and the UTM Zone 11N coordinate systems, respectively, according to the regions of ECP, and then the landcover classes are extracted at the corresponding locations of the ECPs directly.

3.2. Elevation Error Correction Model of SRTM DEM based on PSO-RF

Random forest is a machine learning algorithm proposed by Breiman that can be used to solve nonlinear regression problems. It has the advantages of high accuracy and noise resistance and is not easy to overfit [25]. Therefore, in this study, a RF nonlinear regression model is designed to predict the elevation error of the SRTM DEM. At the same time, considering the influence of hyper-parameters on the accuracy and robustness of the correction model, the PSO algorithm is further integrated to optimize the hyper-parameters of the proposed RF model.

3.2.1. Elevation Error Model of SRTM DEM based on RF Regression

In this study, a SRTM DEM elevation error model based on the RF regression is designed as (1), which has the following six response variables: longitude, latitude, slope, aspect, relief, and landcover class.

$$H_{error} = f_{RF}(Lat, Lon, Sl, As, Re, Gl) \tag{1}$$

Where H_{error} is the elevation error between SRTM DEM and ECPs, *Lat*, *Lon*, *Sl*, *As*, *Re*, *Gl* are the latitude, longitude, slope, aspect, relief and landcover class, respectively.

Based on the above elevation error model, the latitude and longitude information [*Lat*, *Lon*], terrain factors [*Sl*, *As*, *Re*], and landcover class [*Gl*] of the ECPs are used as the input parameters of the model, and the corresponding SRTM DEM elevation errors (H_{error}) to the ECPs are used as the model target, which together constitute the model training set. As shown in Figure 5, based on the Bagging framework [25, 26], multiple decision trees are combined in a parallel manner. The bootstrap sampling method with putback random sampling of the training set is then used to generate a number of sub-training sets for the training of decision trees. Randomly selecting n (n<6) variables from the response variables [*Lat*, *Lon*, *Sl*, *As*, *Re*, *Gl*] as the candidate variables for the node division of the decision tree, for each node, iterate through the selected n variables to divide it. The corresponding variable values j and s of the division will be used as the optimal division variable and division point when the mean square error of H_{error} in these two datasets (named D_1 and D_2) resulting from the division is the smallest and the sum of the mean squared error of the two data sets is also the smallest. In detail, the expression of the cost function is shown as (2).

$$\min_{j,s}\left[\min_{m_1}\sum_{x_i\in D_1(j,s)}(H_{error,i}-m_1)^2+\min_{m_2}\sum_{x_i\in D_2(j,s)}(H_{error,k}-m_2)^2\right] \tag{2}$$

Where m_1 and m_2 are the mean values of H_{error} in the divided data sets D_1 and D_2, respectively, x_i is

ISSN 2616-5767 Vol.6, Issue 11: 70-81, DOI: 10.25236/AJETS.2023.061111

the variable attribute. The training of the random forest elevation error model is completed by dividing the decision tree into several sub-training sets to build different decision trees. Then, the trained elevation error model is used in the prediction of H_{error} results corresponding to the new response variables [*Lat, Lon, Sl, As, Re, Gl*], and the average of the results of each decision tree is used as the final result of the model to obtain the corresponding elevation error.

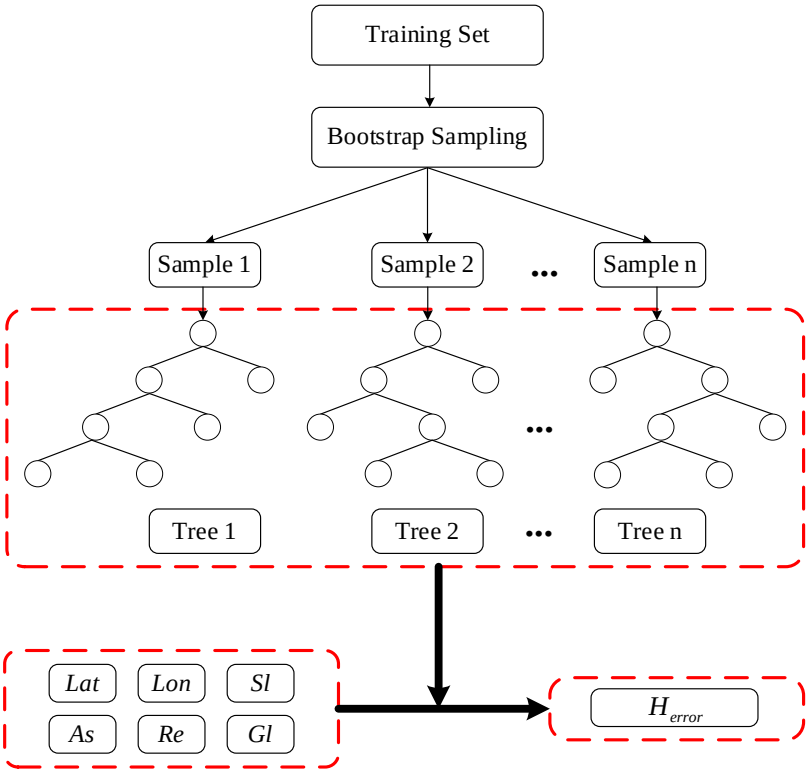

Figure 5: Elevation error model based on Random Forest.

3.2.2. Hyper-parameters Optimization based on PSO

From the above RF training process, it is clear that two hyper-parameters, the number of decision trees (*n_estimators*) and the maximum number of selectable feature variables for node division (*max_features*), are the key points for the model training, and the values of both have a large impact on the model building. To avoid reducing the accuracy of the RF model due to improper parameter setting, the PSO algorithm is used to determine the optimal combination of these two hyper-parameters. Firstly, the population is initialized by integer coding based on the solution space of the two hyperparameters, and then the optimal combination of parameters is searched by comparing the values of the fitness function under different parameter combinations after iterative updates of the velocity and position of particles in the solution space as shown in equation (3).

$$\begin{cases} V_i(k+1) = wV_i(k) + c_1 r_1[p_{best,i}(k) - X_i(k) + c_2 r_2[g_{best}(k) - X_i(k)] \\ X_i(k+1) = X_i(k) + V_i(k+1) \end{cases} \tag{3}$$

where $V_i(k)$ is the velocity of the i_{th} particle in the k_{th} iteration, $X_i(k)$ is the position of the i_{th} particle in the solution space in the k_{th} iteration, w is the inertia weight, c_1 and c_2 are the learning effects, r_1 and r_2 are random numbers in [0-1], $p_{best,i}$ is the position corresponding to the value of the best fitness function experienced by the i_{th} particle, and g_{best} is the position corresponding to the value of the best fitness function experienced by the whole particle population.

Considering the computational efficiency and the searchability of the PSO optimization process, the number of particle swarms is set to 20 and the maximum number of iterations is set to 50 through prior experiments. The inertia weight w in equation (4) is linearly decremented to ensure a better convergence of the algorithm when performing particle velocity calculations, and the decreasing strategy is shown as follow:

$$w = w_s - (w_s - w_e)\frac{k}{k_{\max}} \tag{4}$$

ISSN 2616-5767 Vol.6, Issue 11: 70-81, DOI: 10.25236/AJETS.2023.061111

Where w_s is the initial inertia weight, w_e is the termination inertia weight, k is the number of current iterations, and k_{max} is the maximum number of iterations. Without loss of generality, k_{max} is set to 50, w_s is set to 0.95, and w_e is set to 0.4.

The value of the fitness function in this study is determined using a 5-fold cross-validation of the RF elevation error model. The original training set is randomly divided into five groups, four of which are used for the training of the RF model and one for the validation of the model accuracy, and the mean squared error (MSE) is used for the evaluation index:

$$MSE = \frac{1}{N}\sum_{i=0}^{n-1}(H_{error} - \hat{H}_{error}) \tag{5}$$

Where N is the number of data used for validation, H_{error} is the predicted elevation error of SRTM DEM, and $\hat{H}_{error}$ is the true elevation error. Each group is used for accuracy verification in turn, and the mean value of the 5 times accuracy verification results is used as the fitness function value, and the smaller value of the fitness function means the higher accuracy of the model under this parameter.

3.2.3. The Combination Model based on PSO and RF for SRTM DEM Correction

Combining the above error correction and parameters optimization models, the SRTM DEM elevation error correction model based on PSO-RF is further developed as (6).

$$\begin{cases} H_{correct} = H_{error} + H_{original} \\ H_{error} = f_{PSO-RF}(Lat, Lon, Sl, As, Re, Gl) \end{cases} \tag{6}$$

where $H_{original}$ and $H_{correct}$ are the elevations of SRTM DEM before and after correction respectively.

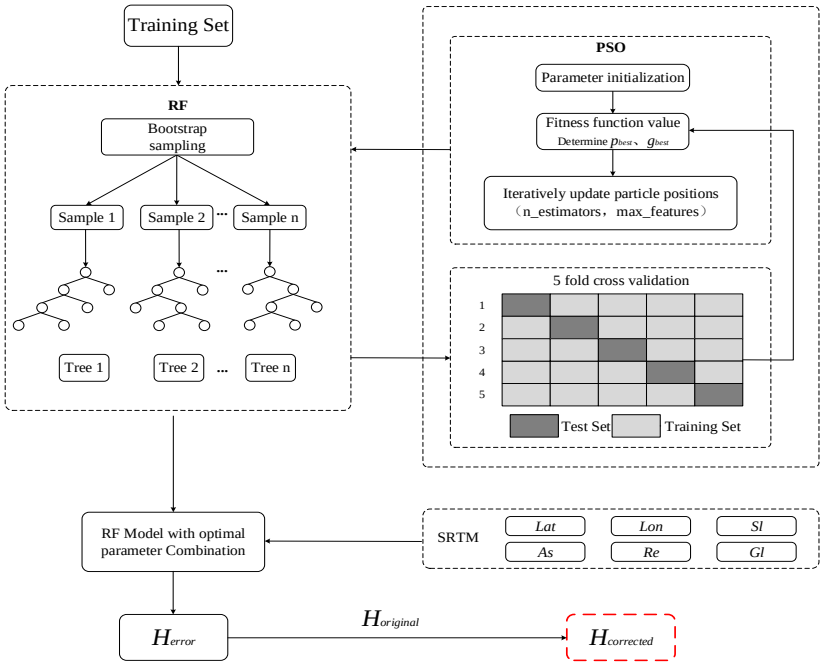

Figure 6: The PSO-RF correction model of SRTM DEM.

As shown in Figure 6, the elevation error model based on RF with the optimal combination of hyper-parameters is trained firstly by fusing parameter optimization of the PSO algorithm using the training set. Then the trained elevation error model is used in the prediction of the H_{error} based on the response variables [*Lat*, *Lon*, *Sl*, *As*, *Re*, *Gl*] corresponding to each SRTM DEM pixel, and then the obtained elevation error is combined with the $H_{original}$ to obtain the $H_{correct}$.

3.3. Accuarcy Assessment

To quantitatively verify the elevation accuracy of the corrected SRTM DEM, the corrected DEM is compared with the original SRTM DEM and airborne-derived LiDAR DEM, and the root mean square error (RMSE), mean absolute error (MAE) are used as validation indexes, these indexes can be calculated as:

ISSN 2616-5767 Vol.6, Issue 11: 70-81, DOI: 10.25236/AJETS.2023.061111

$$RMSE = \sqrt{\frac{1}{N}\sum_{i=1}^{N}(h_i - h_i)^2} \tag{7}$$

$$MAE = \frac{\sum_{i=1}^{N}\left|h_i - h_i\right|}{N} \tag{8}$$

where N is the calculated number of points, h_i is the elevation value to be evaluated for the i_{th} point, and h_i is the corresponding reference elevation value.

4. Results and Discussion

In order to verify the effectiveness and superiority of the PSO-RF model proposed in this study for elevation error correction of SRTM DEM, this study uses the LiDAR DEM range as the main validation area and compares the SRTM DEM corrected by the PSO-RF model with the original SRTM DEM and the SRTM DEM corrected by the PR model for qualitative and quantitative elevation accuracy, respectively.

4.1. Qualitative Analysis

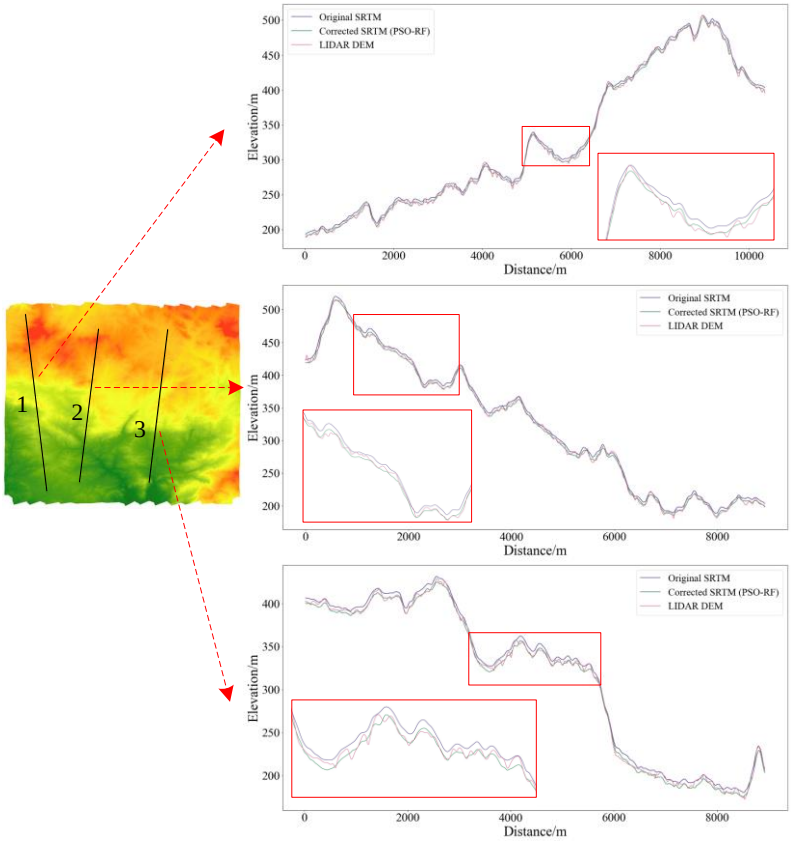

Figure 7: Comparison diagram of elevation profiles.

Firstly, a qualitative analysis is performed by intercepting the elevation profiles of the original SRTM DEM and the SRTM DEM corrected by the PSO-RF model at the location of the black line in Figure. 7. To facilitate the comparison and analysis, the elevation profiles corresponding to the LiDAR DEM, which are more accurate and used as a reference standard, are also shown together. From the details of the red box in the figure, it can be seen that the elevation errors caused by the vegetation and other factors make the elevation profiles of the original SRTM DEM significantly higher than that of the LiDAR DEM, while the SRTM DEM corrected by the PSO-RF model reduces the errors and its profiles are closer to that of the LiDAR DEM. At the same time, due to the large elevation values in the test area, the elevation profiles corresponding to the PR model and the PSO-RF model are close, and it is difficult to judge the

ISSN 2616-5767 Vol.6, Issue 11: 70-81, DOI: 10.25236/AJETS.2023.061111

advantages and disadvantages of the two models only from a qualitative point of view, and further comparison through quantitative calculation is still needed.

4.2. Quantitative Analysis

The elevation points for quantitative accuracy evaluation are extracted from the profiles shown in Fig. 7 at certain intervals, and the elevation values of the original SRTM DEM, corrected SRTM DEM by two models and LiDAR DEM are obtained at the location of these elevation points. The RMSEs of elevation between each SRTM DEM and the LiDAR DEM is calculated using the elevation dates of extracted elevation points, and the calculation results are shown in the scatterplots in Figure. 8. Among them, Figure 8a–c are the results of the original SRTM DEM, the SRTM DEM corrected by the PR model, and the SRTM DEM corrected by the PSO-RF model at line 1 in Fig. 7, respectively, Figure 8d–f are the results of the three SRTM DEMs at line 2, respectively, Figure 8g–i are the results the three SRTM DEMs at line 3, respectively. It can be seen from the Figure 8 that the RMSEs of the corrected SRTM DEMs in the three sets of experiments are significantly reduced compared with the original SRTM DEM, among which the RMSEs and MAEs corresponding to the PR model are decreased by 27.9%, 26.4%, 36.3% and 37.5%,41.8%, 45.3% in the three sets of experiments, respectively, and the RMSEs and MAEs corresponding to the PSO-RF model are decreased by 45.1%, 40.8%, 44.1% and 51.2%, 43.3%, 48.3% in the three sets of experiments, respectively. Table 1 shows the results of elevation accuracy evaluation of all the above points. Compared to the SRTM DEM corrected by the PR model, the RMSE and MAE corresponding to the corrected SRTM DEM corrected by the PSO-RF model are 9.24% and 13.3% lower. The correction performance of the PSO-RF model is better than that of the PR model, which further improves the quality of corrected SRTM DEM.

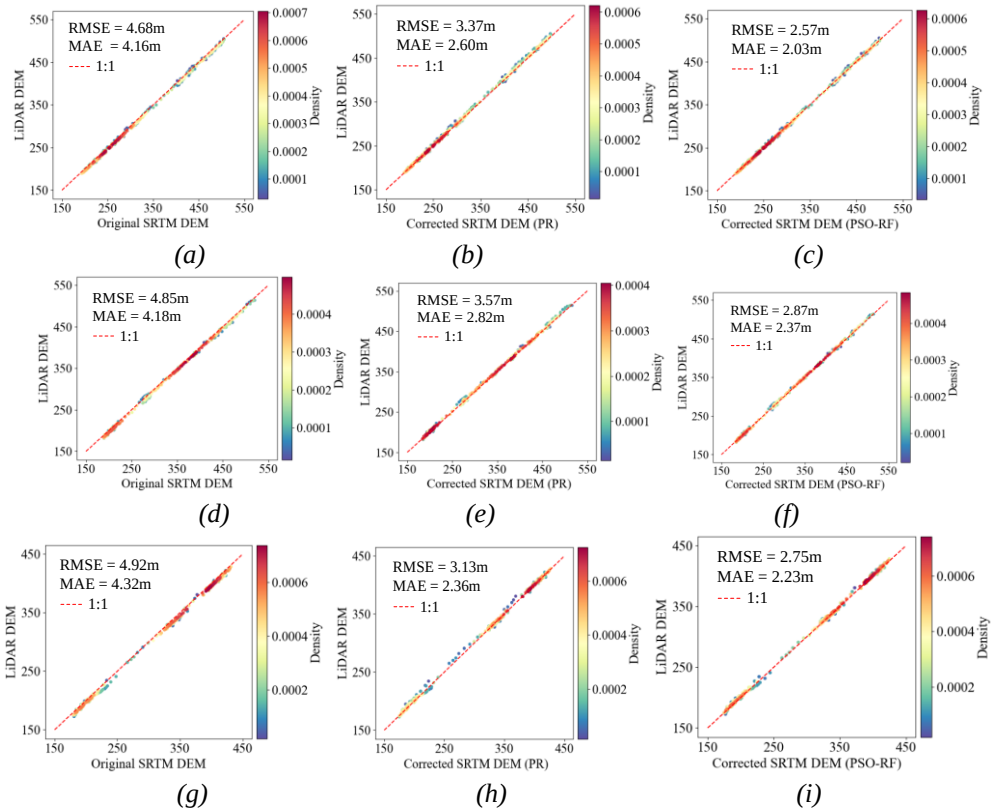

Figure 8: Scatterplots of (a) original SRTM DEM, (b) the SRTM DEM corrected by the PR model, and (c) the SRTM DEM corrected by the PSO-RF model versus the LiDAR DEM at line 1; Scatterplots of (d) original SRTM DEM, (e) the SRTM DEM corrected by the PR model, and (f) the SRTM DEM corrected by the PSO-RF model versus the LiDAR DEM at line 2; Scatterplots of (g) original SRTM DEM, (h) the SRTM DEM corrected by the PR model, and (i) the SRTM DEM corrected by the PSO-RF model versus the LiDAR DEM at line 3.

ISSN 2616-5767 Vol.6, Issue 11: 70-81, DOI: 10.25236/AJETS.2023.061111

Table 1: The results of elevation accuracy evaluation of all the points extracted from the profiles.

SRTM	RMSE/m	MAE/m
Original SRTM DEM	4.81	4.22
Corrected SRTM DEM (PR)	3.36	2.60
Corrected SRTM DEM (PSO-RF)	2.72	2.21

Study also explores the effect of terrain factors and landcover classes on both the original and corrected SRTM DEM. As Tables 2 and 3 demonstrate, elevation errors increase with slope and relief, indicating that the SRTM DEM's elevation error increases with the complexity of terrain. Table 4 reveals differences in elevation errors of SRTM DEM among different ranges of aspect. Furthermore, based on Globeland30, Table 5 calculates the elevation errors of SRTM DEM under different landcover classes, highlighting the largest elevation error in forested regions. Additionally, the PSO-RF model-corrected SRTM DEM demonstrates smaller elevation errors than the PR model-corrected SRTM DEM across various terrains and landcover classes, which means the PSO-RF model displays superior stability to the PR model.

Table 2: The results of elevation accuracy evaluation of SRTM DEM based on slope.

Slope/°	MAE/m			RMSE/m		
	Original	Corrected(PR)	Corrected(PSO-RF)	Original	Corrected(PR)	Corrected (PSO-RF)
0-10	4.51	4.70	2.32	6.58	6.73	1.52
10-20	8.32	7.02	3.35	11.16	9.59	4.76
20-30	8.68	7.69	4.68	11.49	10.32	6.54
30-40	9.95	8.81	6.37	13.31	12.08	9.32
>40	15.45	14.41	11.20	22.62	21.67	17.12

Table 3: The results of elevation accuracy evaluation of SRTM DEM based on relief.

Relief/m	MAE/m			RMSE/m		
	Original	Corrected(PR)	Corrected (PSO-RF)	Original	Corrected(PR)	Corrected (PSO-RF)
0-10	4.03	4.44	1.32	5.80	6.35	1.95
10-20	7.87	6.62	2.91	10.59	9.04	3.98
20-30	8.52	7.29	3.86	11.38	9.90	5.38
30-40	8.70	7.81	4.87	11.56	10.51	6.85
>40	11.05	9.92	7.35	15.60	14.47	11.29

Table 4: The results of elevation accuracy evaluation of SRTM DEM based on aspect.

Aspect/°	MAE/m			RMSE/m		
	Original	Corrected(PR)	Corrected(PSO-RF)	Original	Corrected(PR)	Corrected (PSO-RF)
0-90	6.66	6.14	2.81	10.10	9.21	5.25
90-180	6.15	5.81	2.74	8.99	8.44	4.86
180-270	5.95	5.77	2.69	8.62	8.28	4.51
270-360	7.20	6.55	3.03	10.40	9.43	5.06

Table 5: The results of elevation accuracy evaluation of SRTM DEM based on landcover class.

Landcover class	MAE/m			RMSE/m		
	Original	Corrected(PR)	Corrected (PSO-RF)	Original	Corrected(PR)	Corrected (PSO-RF)
Cultivated Land	2.89	3.79	0.87	3.37	5.43	1.17
Wetland	3.43	4.39	1.18	5.35	6.37	1.95
Artificial Surfaces	4.22	4.06	1.45	5.12	5.61	2.12
Shrubland	5.03	5.39	2.97	7.29	7.76	5.07
Grass Land	5.18	5.26	2.86	7.41	7.71	4.92
Forest	12.49	9.27	3.69	15.25	12.18	5.40

ISSN 2616-5767 Vol.6, Issue 11: 70-81, DOI: 10.25236/AJETS.2023.061111

5. Conclusions

Based on the elevation control photons extracted from ICESat-2/ATLAS, this study integrates multiple categories of elevation error influencing variables such as latitude and longitude, terrain factors, and landcover classes and uses the PSO-RF method to construct an elevation error correction model of SRTM to correct the SRTM in the study area. After the theoretical analysis and experimental comparison analysis, the following conclusions are obtained:

The application of the elevation error correction model constructed by the PSO-RF method to SRTM DEM results in a significant reduction in elevation error with better correction performance compared to the PR model. This outcome suggests that machine learning is better equipped to exploit the nonlinear relationship that exists between SRTM DEM elevation error and its influencing variables. As such, machine learning has certain advantages when it comes to solving problems related to SRTM DEM elevation error correction. We also found that the corrected SRTM DEM still has some elevation errors in several areas, which may be caused by the temporal difference between ICESat-2/ATLAS and the SRTM DEM. Additionally, both the corrected and original SRTM DEMs are vulnerable to certain attribute features, indicating that precision can be enhanced by accounting for these features. Thus, our future work aims to improve the interpolation method by incorporating canopy heights, canopy covers, and other attribute features to achieve more accurate correction of SRTM DEM elevation errors.

Acknowledgments

Many thanks to NASA, USGS, NGCC, and NEON for providing free datasets.

Funding: This research was partly funded by the National Natural Science Foundation of China, grant numbers 41871369, 41901320, 42071439 and 41871295.

Data Availability Statement

The SRTM DEM is available from https://earthexplorer.usgs.gov/. The ICESat-2 ATL03 and ATL08 datasets are available from https://search.earthdata.nasa.gov/search. The Globelan30 data are available from http://globeland30.org/. The airborne LiDAR data can be found on the NEON official website https://www.neonscience.org/.

References

[1] Tsimi C; Ganas A. Using the ASTER Global DEM to Derive Empirical Relationships among Triangular Facet Slope, Facet Height and Slip Rates along Active Normal Faults. Geomorphology. 2015, 234, 171–181.
[2] Ludwig, R; Schneider P. Validation of digital elevation models from SRTM X-SAR for applications in hydrologic modeling. ISPRS J. Photogramm. Remote Sens. 2006, 60, 339–358.
[3] Jafarzadegan K; Merwade V. A DEM-Based Approach for Large-Scale Floodplain Mapping in Ungauged Watersheds. J. Hydrol. 2017, 550, 650–662.
[4] Sun Q; Zhang L; Ding X L; Hu J; Li Z W; Zhu J J. Slope deformation prior to Zhouqu, China landslide from InSAR time series analysis. Remote Sens. Environ. 2015, 156, 45–57.
[5] Shi W; Deng S; Xu W. Extraction of multi-scale landslide morphological features based on local Gi using airborne LiDAR-derived DEM. Geomorphology. 2018, 303, 229–242.*
[6] Tang X M; Li S; Li T; Gao Y D; Zhang S B; Chen Q F. Review on global digital elevation products. National Remote Sens. Bulletin, 2021, 25(1), 167-181.
[7] Gorokhovich Y; Voustianiouk A. Accuracy assessment of the processed SRTM-based elevation data by CGIAR using field data from USA and Thailand and its relation to the terrain characteristics. Remote Sens. Environ. 2006, 104(4), 409-415.
[8] Su Y J; Guo Q H. A practical method for SRTM DEM correction over vegetated mountain areas. ISPRS J. Photogramm. Remote Sens. 2014, 87, 216-228.
[9] Zhao X Q; Su YJ; Hu TY; Chen L H; Gao S; Wang R; Jin S C; Guo Q H. A global corrected SRTM DEM product for vegetated areas. Remote Sens Lett. 2018, 9, 393-402.
[10] Wendi D; Shie Y L; Yabin S; Chi D. An innovative approach to improve SRTM DEM using multispectral imagery and artificial neural network. J. Adv. Model. Earth. Syst. 2016, 8, 691-702.
[11] Du X P; Guo H D; Fan X T; Zhu J J; Yan Z Z; Zhang Q. Vertical Accuracy Assessment of SRTM

ISSN 2616-5767 Vol.6, Issue 11: 70-81, DOI: 10.25236/AJETS.2023.061111

and ASTER GDEM over Typical Regions of China Using ICESat/GLAS. Earth Sci: J China U Geosci, 2013, 38(04): 887-897.
[12] Su Y J; Guo Q H; Ma Q; Li W K. SRTM DEM correction in vegetated mountain areas through the integration of spaceborne LiDAR, airborne LiDAR, and optical imagery. Remote Sens, 2015, 7, 11202-11225.
[13] Qin C C; Chen C F; Yang N; Gao Y; Wang, M N. Elevation Accuracy Evaluation and Correction of SRTM and ASTER GDEM in Shandong Province based on ICESat/GLAS. J. Geo-Inf. Sci, 2020, 22(03): 351-360
[14] Chen C F; Yang S; Li Y Y. Accuracy Assessment and Correction of SRTM DEM Using ICESat/GLAS Data under Data Coregistration. Remote Sens, 2020, 12, 3435.
[15] Zhu X X; Wang C; Xi X H; Nie S; Yang X B; Lin D. Research progress of ICESat-2/ATLAS data processing and applications. Infrared Laser Eng, 2020, 49, 76-75.
[16] Mgruder L; Neuenschwander A; Klotz B. Digital terrain model elevation corrections using space-based imagery and ICESat-2 laser altimetry. Remote Sens. Environ. 2021, 264, 112621.
[17] Rabus B; Eineder M; Roth A; Bamler R. The shuttle radar topography mission—A new class of digital elevation models acquired by spaceborne radar. ISPRS J. Photogramm. Remote Sens. 2003, 57, 241–262.
[18] Farr T G; Rosen P A; Caro E; Crippen R; Duren R; Hensley S; Kobrick M; Paller M; Rodriguez E; Roth L. The shuttle radar topography mission. Rev. Geophys. 2007, 45, RG2004.
[19] Neuenschwande, A; Pitts K. The ATL08 land and vegetation product for the ICESat-2 Mission. Remote Sens. Environ. 2019, 221, 247-259.
[20] Dong J C; Ni WJ; Zhang Z Y; Sun G Q. Performance of ICESat-2 ATL08 product on the estimation of forest height by referencing to small footprint LiDAR data. National Remote Sensing Bulletin, 2021, 25, 1294-1307.
[21] Huang J P; Xing Y Q; Qin L; Xia T T. Accuracy verification of terrain under forest estimated from ICESat-2/ATLAS data. Infrared and Laser Engineering, 2020, 49, 122-131.
[22] Li Y; Fu H G; Zhu J J; Wang C C. A Filtering Method for ICESat-2 Photon Point Cloud Data Based on Relative Neighboring Relationship and Local Weighted Distance Statistics. IEEE Geosci Remote S. 2021, 18, 1891-1895.
[23] Liu X; Zhang L H; Dai Z Y; Chen Q; Zhou Y F. A Parameter-free Denoising Method for ICESat-2 Point Cloud under String Noise. Acta Photonica Sin. 2022, 51, 1110002.
[24] Zhang G P; Xing S; Xu Q; Li P C; Wang D D; Zhang X L; Chen K. Ground Photon Extraction From Photon-Counting LiDAR Data Using Adaptive Cloth Simulation With Terrain Index. IEEE Geosci Remote S. 2022, 19, 1-5.
[25] Breiman L. Random Forests. Mach Learn. 2001, 45, 5-32.
[26] Yang Q Q; Jin C Y; Li T W; Yuan Q Q; Shen H F; Zhang P L. Research progress and challenges of data driven quantitative remote sensing. National Remote Sens. Bulletin, 2022, 26, 268-285.